WPPFC-PR(18) 19305

M Ben Yaala et al.

Quartz micro-balance and in situ XPS study of the adsorption and decomposition of ammonia on gold, tungsten, boron, beryllium and stainless steel surfaces

Preprint of Paper to be submitted for publication in
Nuclear Fusion

This work has been carried out within the framework of the EUROfusion Consortium and has received funding from the Euratom research and training programme 2014-2018 under grant agreement No 633053. The views and opinions expressed herein do not necessarily reflect those of the European Commission.

Quartz micro-balance and in situ XPS study of the adsorption and decomposition of ammonia on gold, tungsten, boron, beryllium and stainless steel surfaces

M. Ben Yaala[1], L. Marot[1], R. Steiner[1], L. Moser[1], G. De Temmerman[2], C.Porosnicu[3], C. Lungu[3], M. Oberkofler[4] and E. Meyer[1]

[1] Department of Physics, University of Basel, Department of Physics, CH-4056 Basel, Switzerland

[2] ITER Organization, Route de Vinon-sur-Verdon, CS 90 046, 13067 St Paul Lez Durance Cedex, France

[3] National Institute for Laser, Plasma and Radiation Physics Atomistilor 409, Magurele, Jud Ilfov 077125, Bucharest, Romania

[4] Max Planck Institute for Plasma Physics, Boltzmannstr. 2, 85748 Garching, Germany

E-mail: marwa.benyaala@unibas.ch

Abstract.

Gas seeding is often used in tokamaks to reduce the power load onto the divertor target plates. Nitrogen is the preferred seeding species because of its favourable radiative properties as well as its apparent beneficial effect on plasma confinement. However, nitrogen molecules are chemically reactive with hydrogen and its isotopes to form stable ammonia compounds. Since ammonia is a polar molecule, sticking on metal surfaces can be expected, increasing as a consequence the tritium retention which could pose a serious risk for ITER operation and maintenance. It is, therefore, important to understand the adsorption mechanism of ammonia on surfaces, investigate when the surface saturation occurs and whether ammonia adsorbs as a molecule or undergoes a dissociation on the surface. In this contribution, ammonia sticking on different fusion-relevant materials is presented. The results show a pressure-dependent ammonia sticking on tungsten, boron and stainless steel followed by a partial desorption from these surfaces while on gold and beryllium, ammonia molecules weakly adsorb and completely desorb. A detailed explanation of the two interaction mechanisms is addressed. Furthermore, the time dependence of ammonia desorption as well as the chemical state of non-desorbed residuals were investigated with X-ray Photoelectron spectroscopy. Tungsten, boron and stainless steel surfaces showed a continuous dissociation process from NH_3 to NH_2, NH, N and surface nitrides.

1. Introduction

In a fusion device, power from the core plasma has to be exhausted by the plasma-facing components, mainly in the divertor area, a special area of the plasma chamber where the open magnetic field lines intersect the primary plasma-facing components and where the plasma is neutralized and pumped away. In ITER, impurities will be seeded into the edge plasma to radiate 75% of the incoming power and reduce heat loads onto the divertor plates to values compatible with the divertor power handling capabilities [1]. Seeding gases that are currently under investigation in divertor tokamaks like JET (Joint European Torus), ASDEX Upgrade (Axially Symmetric Divertor Experiment) and foreseen for ITER are nitrogen (N_2), argon (Ar) and neon (Ne) or a mix of them. N_2 is the preferred seeding species because of its favourable radiative properties [2]. Moreover, N seeding was shown to lead to improved confinement (and hence performance) in full-metal tokamaks such as JET-ILW (JET ITER-Like Wall) and ASDEX Upgrade [3, 4]. Compared with Ar and Ne, N_2 radiates at lower temperature and, therefore, closer to the divertor plates, thus not degrading the confined plasma. However, once dissociated, N atoms chemically react with H and its isotopes (D/T) to form ammonia (NH_3) isotopologues. In ASDEX Upgrade, up to 8% of the injected N_2 was converted into NH_3 [5, 6] and laboratory experiments have shown that even higher levels of N-to-NH_3 conversion (more than 10%) were possible in low-temperature plasmas [7, 8]. The formation of large quantities of tritiated NH_3 has consequences for several aspects of the ITER operation and maintenance. Since NH_3 is a polar molecule, it can be easily adsorbed on metallic surfaces and in particular on ITER first-wall material beryllium (Be), divertor material tungsten (W) and on the vacuum vessel and pipework made of stainless steel (SS). The in-vessel T inventory in ITER is limited to 1 kg [9] for safety reasons and the formation and sticking of large quantities of tritiated ammonia could contribute to the overall inventory while the recovery of T from ND_2T is still an open issue. Furthermore, the formation reaction of ammonia in tokamaks is still and the sticking of the formed ammonia on fusion-relevant surfaces is not fully understood. Quantification of NH_3 sticking is, therefore, of considerable importance and will be studied on Be, W and SS surfaces in this paper. In addition, boron (B) and gold (Au) surfaces will be investigated as well. The former element is largely used in tokamaks to decrease the oxygen (O) content (boronization) [10] while the later can be used as a reference.

In the literature, several studies [11–15] agreed on NH_3 molecule interaction mechanisms with W through chemisorption and decomposition on W surface. On Au surfaces, however, it is still not clear if NH_3 molecules weakly chemisorb or physisorb [16]. On B and Be surfaces, NH_3 sticking was never investigated. Only calculations based on quantum density functional theory (DFT) [17] were performed to investigate molecular and atomic N reactions. In his calculation, A. Allouche *et al.* showed that NH_3 does not stick on a Be surface. On SS surfaces, A. de Castro [18] and Neuwirth [5] indirectly investigated NH_3 sticking by performing a gas balance analysis of NH_3 injected in a SS

vacuum vessel. Even though in both studies strong NH_3 retention was observed, there is still considerable ambiguity with regard to the interaction mechanism of this molecule with the surface. In fact, Neuwirth *et al.* explained the NH_3 interaction with the metal by a decomposition/chemisorption process while de Castro *et al.* claims that at 323 K, a very large number of NH_3 monolayers stick by physisorption (beyond 2000 NH_3 monolayers sticking that corresponds to 39.9 $\mu g/cm^2$ of ammonia molecules retention on the wall). Furthermore, to our knowledge, for all investigated materials, no pressure dependence study was done.

The present paper aims to investigate the interaction of NH_3 molecules with Au, W, SS, Be and B surfaces using a quartz microbalance (QMB) and X-ray photoelectron spectroscopy (XPS) techniques. For that, a detailed explanation of QMB theory and factors affecting its frequency shift will first be presented in section 3, along with a new calibration technique for the QMB. In section 4 a detailed NH_3 adsorption/desorption study will be presented by examining the effect of both pressure and surface material on sticking. Finally, an XPS study to analyse the residual NH_3 molecules sticking on the surface will be presented.

2. Experimental setup

The experiments were carried out in a SS vacuum chamber with a background pressure better than 5×10^{-7} mbar. NH_3 interactions with several surfaces was studied at different pressures in the range of 10^{-3} to 800 mbar. A thin film of the desired elements was first deposited on the QMB surfaces. For that, 20 nm of W, SS (containing 64% of Fe, 12% of Cr, 7% of Ni, 16% of O and traces of Mo, C, Si and Cu)), and B were deposited by magnetron sputtering technique. However, Be deposition (20 nm) was performed by the Thermionic Vacuum Arc (TVA) technique described in [19]. In fact due to the toxicity of Be, the deposition was not possible in our system and was done in INFLPR laboratory in Romania. Only the QMBs deposited with Be were exposed to air while the other materials were deposited and exposed to NH_3 without breaking the vacuum. When the QMB reached a stable frequency (less than 0.1 Hz frequency change per 30 min), NH_3 gas was introduced through a leak valve from the gas line to the vacuum chamber after shutting the valves to pumps. The NH_3 pressure was maintained for 30 minutes while the frequency of QMB was continuously monitored. During this time no wall outgassing effect was seen, i.e. after reaching the constant pressure and stopping the gas inlet no pressure increase was seen however this pressure was slightly decreasing due to the ammonia sticking on the walls. The pressure decrease caused by the SS wall pumping of ammonia was continuously corrected by introducing the gas in the chamber until reaching back the constant pressure. By registering the frequency change of the quartz, the mass of NH_3 adsorbed on the surface can be determined using the method described in the section 3. A gas desorption step was then done by pumping the gas from the chamber and measuring the resulting frequency. After the desorption process, samples were transferred without breaking the vacuum to the XPS chamber for chemical

analysis at several time intervals.

To verify the reproducibility of the results, all measurements on W surfaces were performed twice and two adsorption/desorption cycles were repeated for SS, B and Au for one fixed pressure. Furthermore, to verify the accuracy of each new installed QMB crystal, an Ar cycle at 50 mbar was done before each experiment. The standard error measured was equal to 0.09 Hz which indicates the accuracy of the QMB technique for our measurements. The error bars shown in Figure 5 were calculated by taking the two above mentioned points into account (50 mbar Ar cycle and experiment repetition). The QMB crystals used are AT-cut piezoelectric quartz crystals (6 MHz resonance frequency) with deposited Au electrodes purchased from Inficon. The QMB was connected to a 6 MHz oscillator circuit (Inficon OSC-100 Oscillator). A frequency counter (Agilent 53132A Universal counter) was used to monitor the QCM oscillation frequency.

For the XPS characterization, samples chamber were transferred without breaking the vacuum. The ultra-high vacuum (UHV) chamber is equipped with a monochromatic Al-Kα X-ray source (hν=1486.6 eV) and a photoelectron spectroscopy analyzer (VG ESCALAB 210) with an energy resolution of 0.5 eV at 20 eV pass energy. The Au 4f7/2 peak was set to 84 eV for electron binding energy (BE) calibration. Fitting of the core level lines was performed using DoniachSunjic functions [20] after a Shirley background subtraction [21], using UNIFIT for Windows (Version 2015) software [22]. The intensities were corrected using Scofield sensitivity factors and the transmission function measured with our system as described in [23].

To characterize the roughness of the bare crystals before deposition and also of the deposited layers, a Tencor 500 alpha stepper was used. The average roughness (R_a) was obtained by averaging 10 measurements of 1 mm length.

3. Parameters influencing the frequency change of a QMB

3.1. QMB Theory

Measurement of the frequency change of a crystal due to the mass loading, Δf_m, is the fundamental principle of operation of QMBs. However this frequency change is not only affected by the mass change but by 4 other factors. These factors can be classified into two groups; namely the physical parameters of the surrounding gas and the structural parameters of the crystal. The former includes the temperature, pressure, viscosity, and density of the surrounding fluid, whereas the latter involves the mass loaded on the crystal and the surface roughness of the crystal. The total frequency shift of the QMB can be written in the form:

$$\Delta f = f - f_0 = \Delta f_m + \Delta f_T + \Delta f_P + \Delta f_\nu + \Delta f_r \quad (1)$$

where Δf is the shift of frequency from the fundamental value f_0, f is the measured frequency of quartz, Δf_m, Δf_T, Δf_P, Δf_ν and Δf_r are frequency shifts related to mass loading, temperature change, pressure change, density/viscosity of the surrounding fluid and the roughness of the QMB surface respectively.

The response of the QMB to thermal changes was neglected in this work. In fact, the effect of temperature variations in the range of 15–45 °C on the AT cut quartz crystal used is less than 0.1 Hz/hour. As all our experiments were done at room temperature (RT) (that varies at a maximum of 0.8 °C/day as measured) and a full pressure cycle measurement last less than 8 hours (so a maximum of 0.8 Hz frequency shift), temperature effect on the QMB oscillation will be neglected i.e. $\Delta f_T = 0$.

The mass effect on the QMB frequency was first derived by Sauerbery [24] and is given by:

$$\Delta f_m = \frac{-2nf_0^2}{(\rho_q \mu_q)^{\frac{1}{2}}} \Delta m = -C_m \Delta m \tag{2}$$

Where n is the number of faces of the crystal in contact with the gas, ρ_q the density of the quartz ($\rho_q = 2.648$ g/cm^3), μ_q the shear modulus of quartz ($\mu_q = 2.947\times10^{11}$ g/cm.s^2), Δm the change in mass per unit area and C_m the mass sensitivity of the QMB. For our experiment, the gas is in contact with both sides of the QMB and n is thus fixed to two for Au bare crystals. For other materials (SS, W, B and Be), as the coating was done only from one side of the crystal, n is fixed to 1 and the mass of ammonia adsorbed on the Au back side was substacted from the total mass.

Both Δf_P and Δf_ν terms are associated with the influence of the medium surrounding the quartz crystal. The effect of pressure can be described as the frequency change due to the hydrostatic pressure exerted on the crystal by a hypothetical gas of zero density. It represents the compression effect of an increasing pressure of the surrouding gas on the quartz crystal. Stockbridge [25] showed that the frequency increases linearly with increasing pressure (P) for the case of gases up to pressures of 1 bar and can be written as:

$$\Delta f_P = f_0 \alpha P = C_P P \tag{3}$$

where α is the proportionality constant and C_P is the pressure sensitivity of the crystal. Both terms are independent of the type of fluid in contact with the crystal. Considering the value of α proposed by Stockbridge for a 6 MHz resonating crystal, the C_P calculated is equal to 6.28×10^{-3}. The density (ρ_f) and viscosity (η_f) of the surrounding fluid increase with increasing pressure at a given temperature, leading to an amplitude damping of the oscillating QMB and consequent frequency decrease. Kanazawa and Gordon [26] quantified the relation between the frequency shift (Δf_ν) and the viscosity and density of the surrounding fluids:

$$\Delta f_\nu = \frac{-nf_0^2(\rho_f \eta_f)^{\frac{1}{2}}}{(\pi f_0(\rho_q \mu q))^{\frac{1}{2}}} \tag{4}$$

While Δf_m, Δf_P and Δf_ν can be calculated directly using equations 2, 3 and 4, an analytical equation to precisely calculate Δf_r cannot be found in literature. Because of the non-uniform morphology of the surface, gas will be trapped in the crevices of the crystal surface and increase the mass loading on the surfaces. In most experimental work published so far, the roughness effect was not taken into account and only few

papers [27–29] have addressed the problem of quantifying the contribution from the roughness to the total frequency shift. However, it was found that surface roughness can drastically affect the resonance frequency of quartz crystal in contact with fluids [28]. In the next part the method employed to derive Δf_r will be presented.

3.2. Experimental methods for the determination of the frequency shift due to roughness

Herein, we present a calibration method using non-adsorbing noble gases that will allow extracting the frequency shift caused by the sample roughness. Based on the ideal model for surface roughness from Urbakh *et al.* [30–32], and using a perturbation theory model for a slowly varying roughness surface [31, 32], Δf_r can be written in the form:

$$\Delta f_r = -0.5 C_m C_r \rho_f \tag{5}$$

The slowly varying roughness condition for which this equation is applicable is valid when both the average lateral length of surface shapes (ridges and valleys) and the decay length (defined in [28]) is higher than the average height of the surface shapes.
In order to calculate Δf_r in equation 5, the value of the roughness factor C_r should be determined. As shown in [28], for the particular case where the density of the adsorbing gas on the QMB is less than 0.2 g.cm^{-3} and the QMB roughness value is in the range of few nanometers to approx. 700 nm, C_r can be written as:

$$C_r = a_1(1 + b_1 \rho_f) \tag{6}$$

where a_1 and b_1 are the constants assumed to be independent of the gas type and the surface material.
The QMBs used in this study, either bare rough Au coated crystals (as received from the manufacturer) or coated with 20 nm W, SS, B or Be, had R_a comprised between 300 and 465 nm. Also, for our working conditions, i.e. temperature and pressure, and for all gases used in this work, density values do not exceed 0.015 g.cm^{-3}. Therefore, equation 6 can be applied.

Replacing C_r in equation 5, Δf_r can be written as a second order polynomial as function of the gas density:

$$\Delta f_r = -0.5 C_m C_r \rho_f = -0.5 C_m \rho_f (a_1(1 + b_1 \rho_f)) = B_1 \rho_f + B_2 \rho_f^2 \tag{7}$$

To determine B_1 and B_2 values, we measured Δf_r for 3 noble gases Ar, He and Ne on a bare gold crystal. As these gases cannot adsorb at RT on any surface we can consider $\Delta f_m = 0$ and measure the total frequency shift. Then Δf_r is calculated directly by subtracting pressure and viscosity terms from the total frequency shift (see equation 1). Δf_r is plotted in Figure 1 as function of the gas density. Using a second order polynomial fit, B_1 and B_2 coefficients were extracted, allowing one to calculate Δf_r for NH_3 gas.

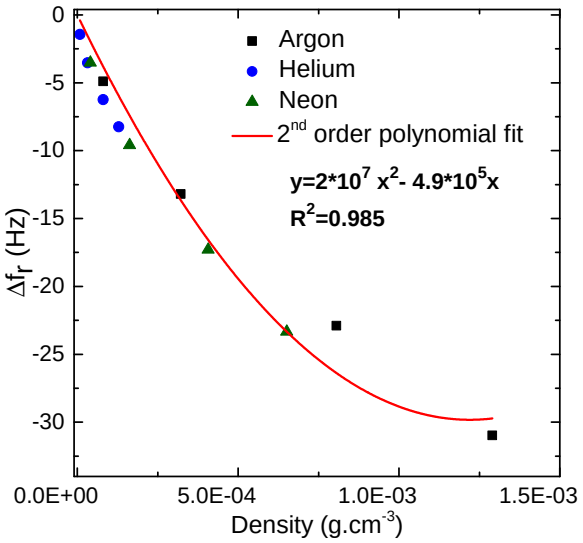

Figure 1: Frequency shift caused by the crystal surface roughness as function of gas density measured for Ar, He and Ne on Au surface fitted with a second order polynomial.

4. Results and discussion

4.1. Interaction of NH_3 with different materials

NH_3 adsorption/desorption cycles done at 50 mbar will first be presented on Au and W surfaces and compared to a reference Ar adsorption/desorption cycle done on Au (non-reactivity and zero adsorption at RT). The results of adsorption cycles of (a) Ar on Au bare crystal, (b) NH_3 on Au bare crystal and (c) NH_3 on W coated Au crystal are shown in Figure 2. The QMB total frequency shift as a function of time is represented by the black curve while the blue dashed line represents the calculated sum of Δf_P, Δf_ν and Δf_r. As can be seen, the sum of the three terms is higher for Ar than NH_3 due to the higher density of Ar ($\rho_{Ar} > \rho_{NH3}$). In fact, while Δf_P does not depend on the gas nature, Δf_ν and Δf_r both increase with the gas density. The typical behaviour of a non-adsorbing gas ($\Delta f_m = 0$) is shown in Figure 2a. A sudden frequency decrease is observed when Ar was introduced. The vertical slope corresponds to the phase when the gas pressure is rising until reaching the constant value of 50 mbar. As the desired pressure is attained, the total frequency variation stabilizes and corresponds to the sum of pressure, roughness and viscosity effects on the QMB (blue dotted line). By pumping the gas from the vacuum chamber, these effects disappear and the QMB returns to its initial resonance frequency. As seen in Figure 2b, NH_3 exhibits a different trend on Au. The total frequency shift is much higher than the sum of Δf_P, Δf_ν and Δf_r. According to equation 1, this observation indicates that the observed frequency is mainly due to adsorbed mass on the surface. When the gas was fully pumped from the chamber, the QMB returns to its initial resonance frequency value, indicating a total desorption of NH_3 molecules from the Au surface. The QMB coated with W behaves differently as

can be seen in Figure 2c. In fact, the measured total frequency shift caused by the NH_3 adsorption is around 3.5 times higher on W than on Au indicating that more NH_3 can adsorb on the W surface. Moreover, after the pumping of the chamber, the initial resonance frequency was not reached and, as the base pressure is recovered, there is no residual NH_3 in the vacuum chamber. This indicates that the partial frequency recovery can only be caused by remaining NH_3 molecules on the QMB, i.e. a partial NH_3 desorption.

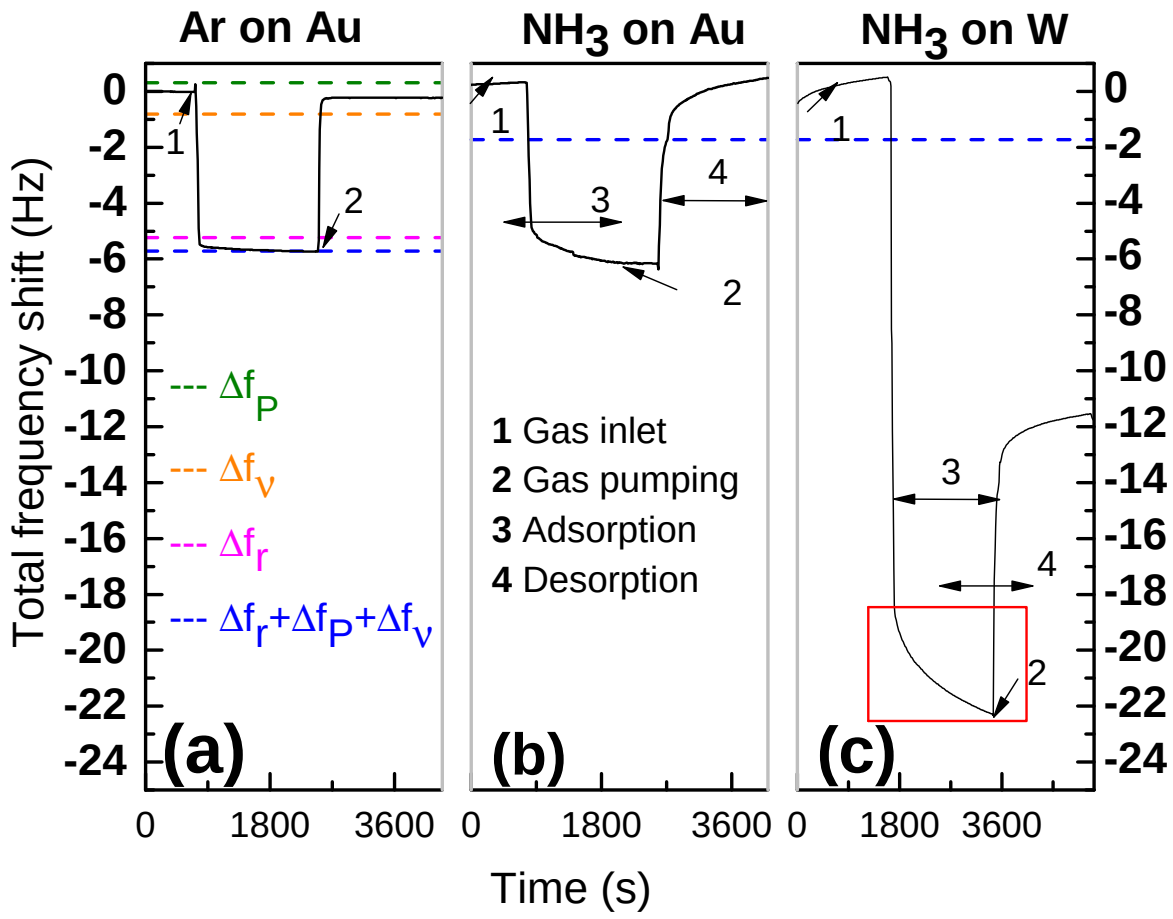

Figure 2: Total frequency shift as a function of time for adsorption/desorption cycle at 50 mbar of a) Ar on Au, b) NH_3 on Au and c) NH_3 on W surfaces.

Taking a closer look on the adsorption phase, one can notice that even though the pressure reached the desired value, the frequency continues to decrease for NH_3 on Au or W with different slopes depending on the material. For clarifications, this phase was highlighted in Figure 2c with a red box. The slope is steeper on W than on Au surfaces, probably because of different adsorption kinetics of NH_3 molecules on those surfaces. More information could be obtained by applying and adjusting a kinetic model to our results. Over the years, a wide variety of kinetics models have been proposed (Langmuir, Pseudo order 1, Pseudo order 2, Pseudo order n, Elovich, Crank, Boyd, Bangham, Weber and Morris...) [33] but none were used in this work as kinetics do

not represent the main focus of this study. Yet, the adsorption equilibrium was not reached during the 30 min of exposure time and it is important to quantify the amount of NH_3 molecules that is missing compared to the equilibrium case. By fitting the total frequency shift during NH_3 adsorption on W with an exponential function, as shown in figure 3, it was found that the difference between the experimental frequency shift due to NH_3 adsorption on W after 30 minutes and the calculated frequency shift at the equilibrium from fitting is equal to 0.24 Hz. This value corresponds to approx. 1% of the total frequency shift measured after introducing the gas at 50 mbar. We can, therefore, assume that after 30 minutes, the adsorption is close to steady state.

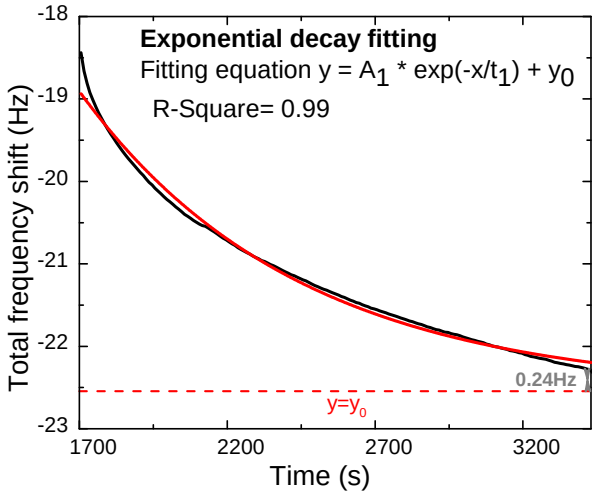

Figure 3: Total frequency shift as a function of time following NH_3 adsorption at 50 mbar on W surface for 30 min. Red curves represents an exponential decay fitting for the measurement points.

In order to explain the difference in NH_3 sticking between the studied materials we refer to their electronic structure. NH_3 molecules possess an electron lone pair available for bonding and adsorption on surface atoms through charge exchange leading to the formation of a true chemical covalent bond. The strength of this bond is directly affected by the empty atomic orbitals on the surface as reported by Gundry and Tompk [34].

On Au surfaces, NH_3 interaction is described as a weak chemisorption [35–38] arising from electron transfer from the NH_3 lone pair orbital to the partially filled Au s band. Yet calculations done by Ante Bilic *et al.* [16], based on DFT showed that the charge transfer from NH_3 to Au is minimal and the local densities of states and the charge distribution provide indication of poor covalent bonding, i.e. a dispersive interaction. Beside this dispersive and/or weak chemisorption of NH_3 on the Au surface atoms, the low mass adsorption measured on gold, in our case, can be explained by another weak interaction. It consists of the NH_3 interaction via one of its H atoms to an O atom adsorbed on the surface [39]. XPS measurements (presented later in section 4.3) of Au coated QMB before NH_3 exposure showed that 11% of the Au surface atomic composition is adsorbed O. Therefore, the weak interaction of NH_3 on Au can also be explained by H bond between NH_3 and surface O atoms.

On the other hand, NH_3 strongly chemisorbs on electron acceptor surface atoms such as W with 4 electrons in the d orbitals, explaining the strong absorption seen in Figure 2. It has to be pointed out that oxygen (from H_2O mainly) is also present on the W surface and can interact with ammonia via H bond but the strong covalent bond between the metal and nitrogen of ammonia is the dominant interaction.

The NH_3 adsorption showed that depending on the nature of the surface, NH_3 can adsorb in mainly 2 different ways: (i) weak interaction consisting of a weak chemisorption and/or dispersive interaction with Au atoms and/or a H bonding to the surface O atoms. The three interactions are weak bonding and can be broken when pumping the gas from the surface, explaining, therefore, the complete desorption of NH_3 from Au and (ii) a strong interaction where NH_3 molecules stick on the surface via electron sharing involving NH_3 lone pairs and the partially filled surface material valence bands. This results in a strong chemical bond and an incomplete desorption of the gas molecules from the surface after pumping.

4.2. Pressure effect on NH_3 adsorption/desorption process

In order to investigate the effect of pressure on NH_3 sticking, consecutive cycles of NH_3 adsorption/desorption on Au, W, SS, B and Be (oxidized surface) were carried out with pressures ranging from 1×10^{-3} to 800 mbar. The results of such consecutive cycles are shown for a W surface in Figure 4 and three main trends can be observed: (i) the total frequency decrease following the gas inlet (Δf) is higher for each cycle at higher gas pressure, suggesting that the NH_3 uptake increases with the pressure, (ii) the frequency shift after the gas pumping i.e the non-desorbed mass remains larger for a higher pressure and (iii) no saturation was reached up to 800 mbar.

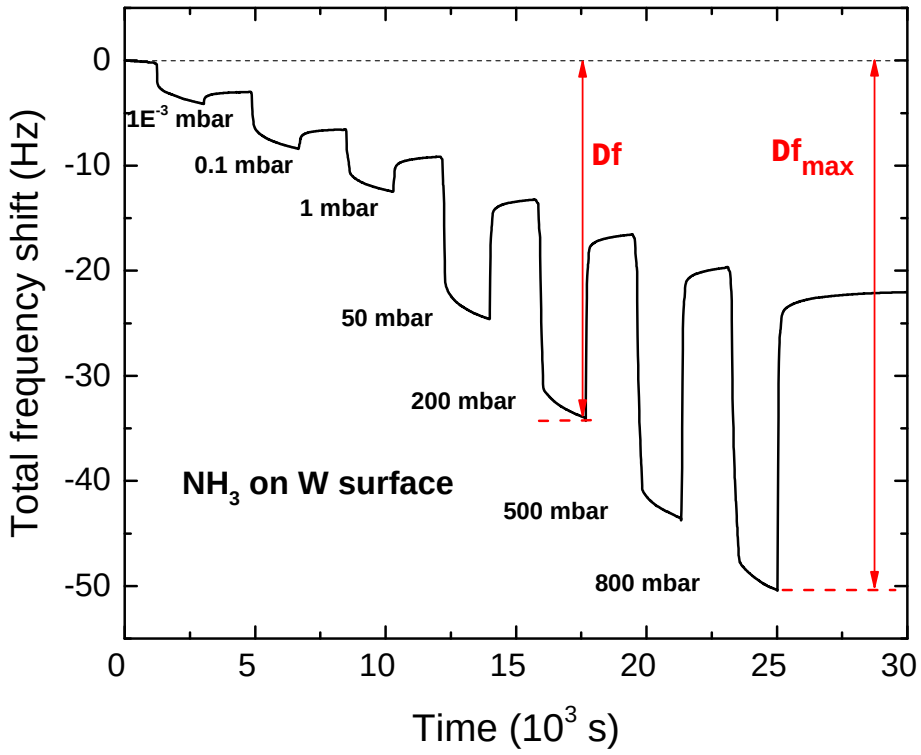

Figure 4: Total frequency shift Δf as a function of time for the adsorption/desorption consecutive pressure cycles of NH_3 on a W surface.

The frequency change for each pressure was then extracted and the maximum value of the NH_3 adsorbed mass was calculated according to the procedure described in section 3, after subtracting the roughness, viscosity and pressure effect. In order to convert this mass uptake into a number of monolayers (ML) adsorbed on the surface, the following calculations were done. Assuming one ML is equal to 6.2×10^{14} molecules/cm^2 [18], the number of ML adsorbing on a surface can be calculated by dividing the number of gas molecules per surface area N_{NH3} by one ML. N_{NH3} can be calculated using the following equation:

$$N_{NH_3} = \frac{\Delta m}{M} \times N_A \tag{8}$$

where M is the gas molar mass and N_A is the Avogadro number. We should note however that the number of ML can be overestimated as we assume a flat surface and neglect the effect of surface irregularities (steps, kinks...) on adsorption. Figure 5 represents the mass and number of ML of NH_3 adsorbed on Au, Be, B, SS and W surfaces.

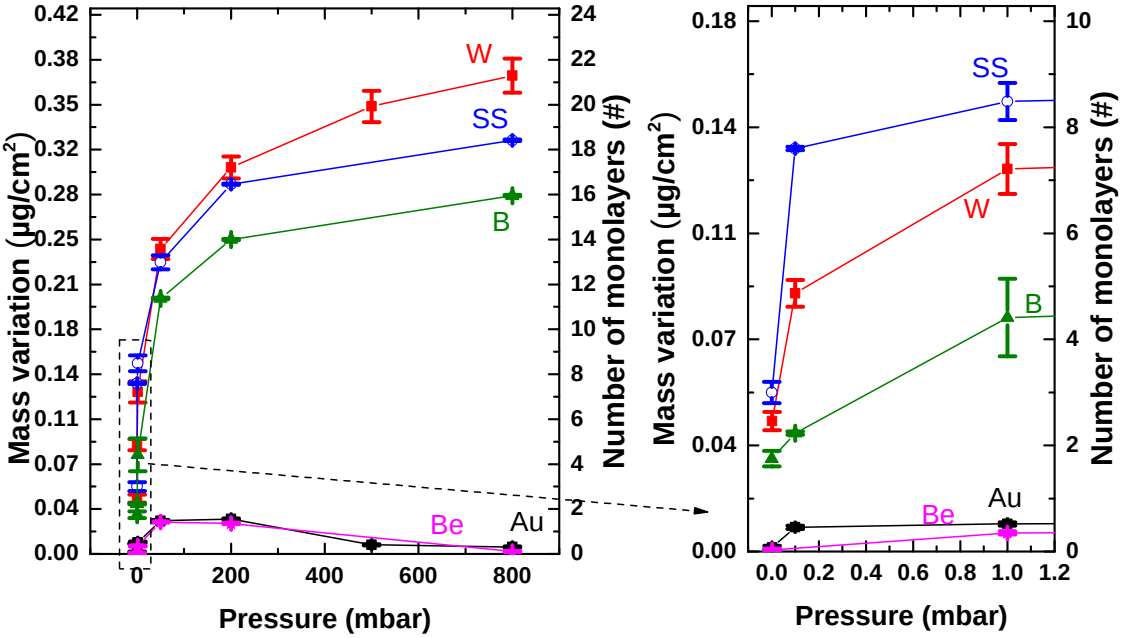

Figure 5: NH_3 mass and number of ML adsorbed on W, SS, B, Au and Be surface after 180 sec of ammonia exposure as a function of pressure.

Adsorption mechanism on Be, B and SS From Figure 5 two major interaction types are observed: a low mass uptake for NH_3 on Be and Au surfaces that does not exceed 2 ML and a high adsorption for W, B and SS. As done earlier for Au and W in section 4.1, the interaction mechanisms of NH_3 on Be, B and SS can be explained and classified in two categories. For SS and B surfaces, NH_3 interaction exhibits a similar behaviour as W consisting of a high adsorption and a partial desorption. On the other hand, NH_3 adsorption on Be surface was observed to be equal to NH_3 adsorption on Au.
For Be, the highest occupied orbital s is filled, making the surface non-reactive to NH_3. A. Allouche *et al.* also confirmed that NH_3 does not adsorb on the Be surface [17]. Yet, in our experiment, NH_3 was found to adsorb on Be and can be explained by the presence of O on the surface. XPS measurements revealed 42% of O on the Be surface (both adsorbed and bonded to Be atoms forming oxides) and NH_3 is known to bind to adsorbed O or to the metal atom for BeO [39]. It should be noted that in the tokamak and precisely in the erosion zone Be will be only in metallic state. As for Au, NH_3 is weakly bound to the Be surface and can be fully desorbed when pumping the gas from the vacuum chamber. Similarly to W, the three main constituents of SS, i.e. Cr, Fe and Ni possess electrons in the d orbitals (respectively 5, 6 and 8) and NH_3 can thus strongly chemisorbs on this electron acceptor surface. The pressure dependence of the adsorption on the SS surface observed in figure 5 (higher than W for low pressure less than 1 mbar and lower than W at high pressures) cannot be explained yet.
Regarding B, NH_3 interacts with the surface through a strong covalently bonded Lewis

adduct where the electron deficient B atoms represent the Lewis base and NH_3, with its lone pair, plays the role of Lewis acid adsorbate. On SS and B surfaces, NH_3 is thus strongly adsorbed and is only partially desorbing when the gas is pumped from the vacuum chamber.

Pressure dependence For Au and Be, the mass uptake increases with pressure until 200 mbar and then decreases for higher pressures which is still not understood. For W, SS and B, the adsorbed mass increases with the NH_3 pressure and no saturation was reached up to 800 mbar. At least 16 ML were measured for B, SS and W surfaces at 800 mbar, indicating the formation of a multi-layered system. To explain the formation of this system, the following mechanism is proposed: the chemical bond formed from the strong interaction between the NH_3 molecules and the surface results in the polarization of the N-H bond of the first NH_3 layer, leading to the formation of a second layer with a strong H bond and consecutively for further top layers. Figure 6a illustrates this suggested mechanism where we present three intermolecular H bonds (red dashed bond in the figure) between NH_3 molecules from each single layer. The decomposition fragments of NH_3 shown in the same figure will be discussed in section 4.3.

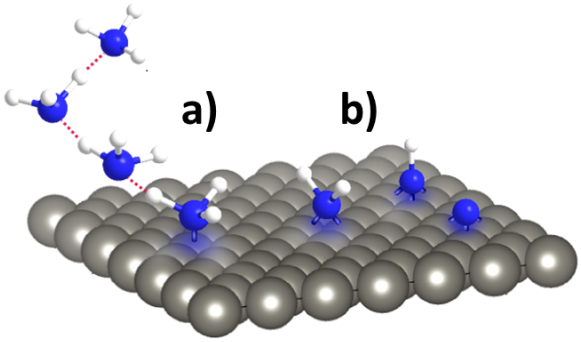

Figure 6: a) Multilayer formation of NH_3 on the W surface through H bonds and b) NH_3 decomposition species on surface. N and H atoms are respectively represented in blue and white. The red dashed lines represent intermolecular H bounds.

The multilayer formation mechanism was already proposed by D.R. Jennison *et al.* for NH_3 adsorption on Pt surface [40]. They have calculated an H bond energy of 0.38 eV between the first and second layer of NH_3 molecules, almost three times higher than that of the gas phase NH_3 dimer $(NH_3)_2$. When NH_3 chemisorbs to Pt it donates electrons from the electron lone pair of the N atom to the empty Pt orbitals. The resulting increased polarization of the NH bonds in the first layer of NH_3 molecules allows a second layer of NH_3 molecules to form unusually strong H bonds. Furthermore, the multilayer formation of NH_3 was shown previously on W [12], Ru [41, 42], ZrB_2 [43], Ni [44, 45] and SS [18] by different techniques.

In the next section, XPS analysis of the non-desorbed NH_3 will be presented.

4.3. XPS study of non-desorbed NH_3

After the desorption process, samples were immediately transferred to the XPS chamber without breaking the vacuum. In Figure 7, the N1s core level spectra of Be and Au surfaces before ammonia exposure (only for Be, was not measured for Au) and after the last NH_3 absorption/desorption cycle (see Figure 4) is presented. As can be seen, no N peak was observed, indicating the absence of NH_3 on both surfaces confirming, therefore, the total desorption discussed in sections 4.1 and 4.2.

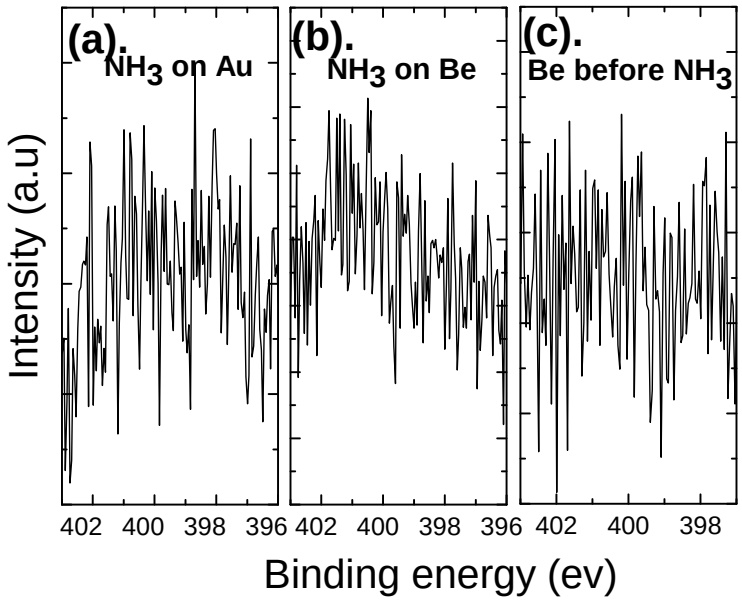

Figure 7: N1s core level spectra recorded 30 min after NH_3 desorption from a) Au surface and b) Be surface.

For the other materials subject to strong NH_3 adsorption, i.e. B, W and SS, XPS measurements performed before and after exposure of NH_3 are shown in Figure 8. The B surface (Figure 8a) was composed of B (77.8 %), O (3.4 %), C (17.6 %) and N (1.2 %). The presence of N and C in the film is due to the fact that B atoms can easily catch species present on the vacuum vessel walls during deposition. The B was either in the form of a carbide B_4C (187.4 eV) or of a nitride BN (190.4 eV) or bound to other B atoms (188.4 eV) [46]. After exposure the N atomic percentage more than doubled from 1.2% to 2.7%, highlighting the bonding of NH_3 to the surface. I has to be pointed out that this increase can not be related to the number of ML observed in section 4.2 as XPS measurement were done after the chamber pumping (ammonia desorption from the sample) and sample transfer. On the other hand, despite the presence of O and carbon (C) on the surface no BCNO (at 191.9 eV) nor BO (at 192–192.7 eV) [47] were measured.

On the SS surface, Cr2p, Fe2p, and Ni2p core level spectra were measured before

and after NH_3 exposure. No change in Ni and Fe peaks were observed and this is probably due to the preferential reactivity of ammonia only with the highest electron acceptor metal of the SS which is the Cr (6 valence electrons missing compared to 4 and 2 for Fe and Ni respectively). Cr2p peak is, therefore, shown in Figure 8c. Before NH_3 exposure, the Cr was measured in a metallic state (Cr^0 at 574.2 eV) and in two different oxidic states: Cr^{+3} in Cr_2O_3 (576.2 eV) and Cr^{+6} in CrO_3 (578.2 eV) [48]. After NH_3 exposure, another peak was identified at 575.1 eV and could be assigned to Cr bound to N (CrN, Cr_2N or CrN_xO_y) [49,50]. This hypothesis is further supported by the absence of changes in the O1s core level spectra, indicating that the Cr peak at 575.1 eV is a sign of Cr-N bonding rather than Cr-O bonding.

The W surface was fully metallic before NH_3 exposure as shown in Figure 8c ($W4f_{7/2}$ at 31.1eV) [51]. W exposure to NH_3 resulted in the formation of W nitride with a peak assigned at 32 eV [52]. Similarly to B, no W oxides were measured at the surface despite the presence of 10% O on the surface, indicating that the O is only adsorbed on the surface and not bonded to W atoms [53]. Furthermore, no oxonitrides peaks were observed at 33.5 eV ($W4f_{7/2}$) and 35.71 eV ($W4f_{5/2}$) [54].

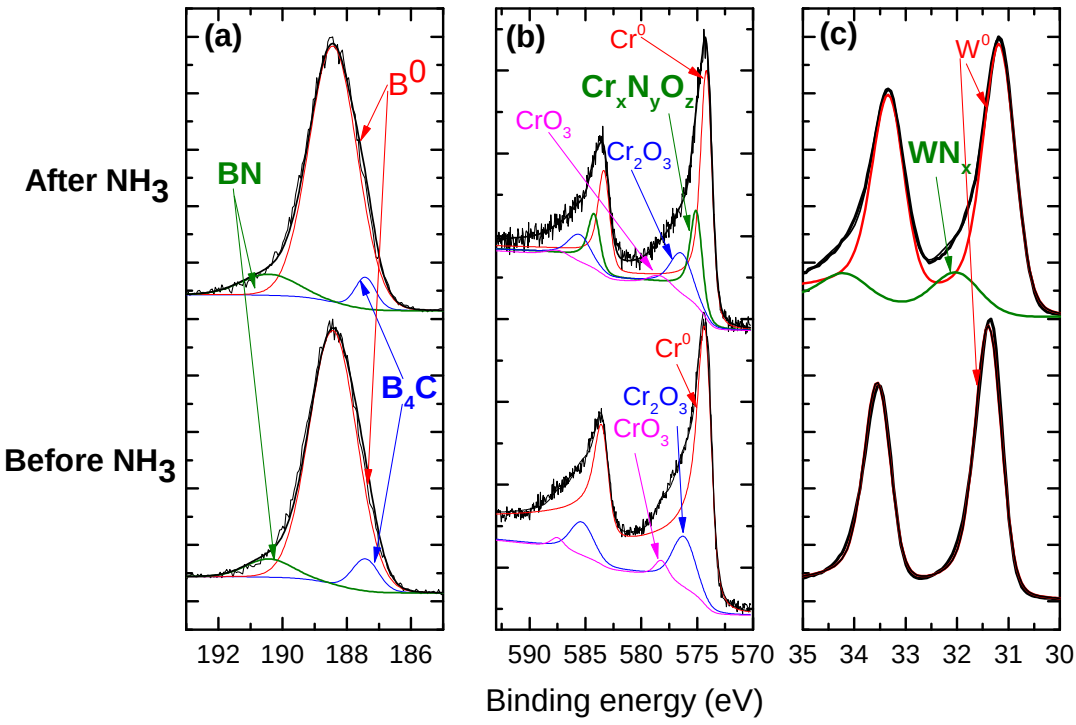

Figure 8: B1s, W4f and Cr2p core levels spectra recorded before NH_3 exposure and 30 min after NH_3 desorption from a) B surface, b) SS surface (only Cr is shown) and c) W surface. The red, green, blue and magenta solid curves are the individual chemical states. Solid black curves are the raw data and the sum curves.

In addition to XPS measurements performed 30 min after NH_3 exposure, N1s core level spectra were recorded at different time intervals ranging from 30 min to one week after the NH_3 exposure. In between measurements, the samples were kept in the XPS vacuum chamber at 10^{-10} mbar. Results are shown in Figure 9 and the measured binding energy (BE) of the different chemical species are summarized in Table 1. B was the sole surface containing N before the NH_3 exposure with 2 peaks located at 397.8 and 399.0 eV, the former corresponding to CN and the latter resulting from B-N bounding.

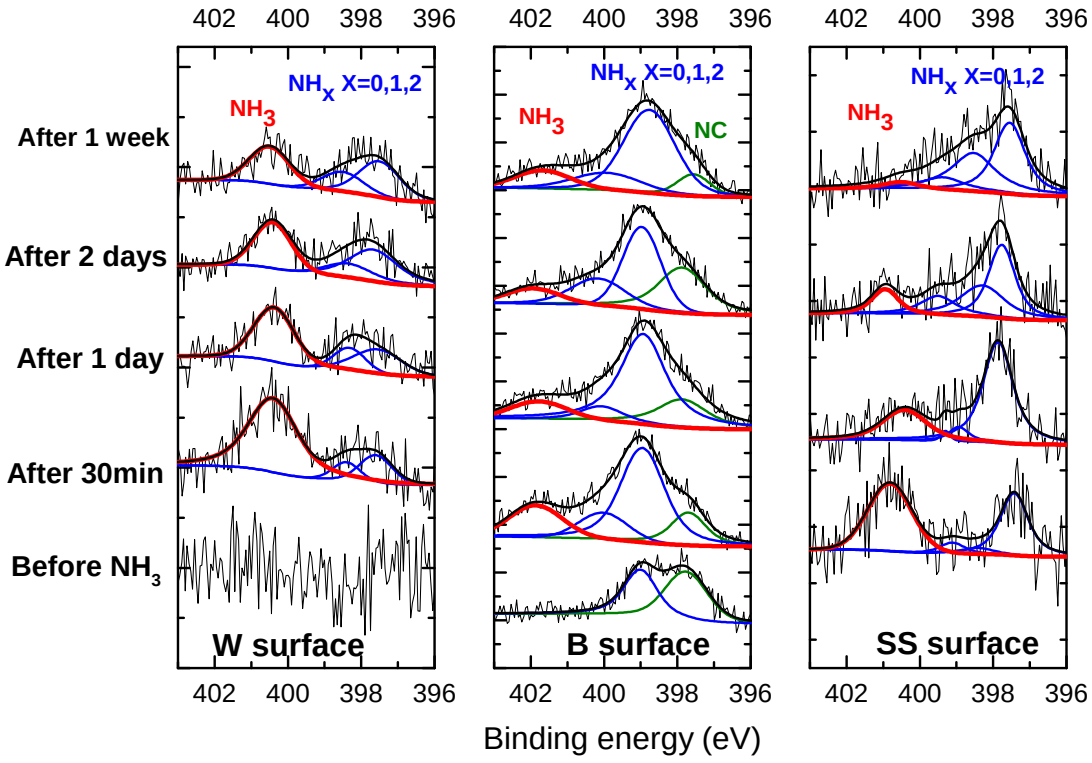

Figure 9: N1s core level measurements for the W, B and SS surfaces performed before and after NH_3 exposure. The red curves are the individual peaks assigned to NH_3 while the blue curves stand for the individual peaks assigned to NH_x (x = 0, 1 and 2). The black curves are the raw data and the sum curves.

After NH_3 exposure, the N1s core level spectra on the W surface can be decomposed in three peaks corresponding to a second layer of NH_3, NH_2, NH and/or surface nitrides (see Table 1). With ongoing waiting time, the decomposition products of NH_3, e.g. NH_x (where x = 0, 1 and 2), saw their peak intensities increase while the peak intensity of NH_3 decreases, indicating a continuous decomposition of NH_3 on the W surface. A similar decomposition process was found on the B and SS surface. All the peaks were identified to be NH_3 and its decomposition products (except for CN on B surface at 397.7 eV), and the corresponding BE are given in Table 1.

Table 1: N1s BE values extracted from XPS measurement on W, B and SS surfaces after NH_3 exposure. Reference values from literature and the corresponding species were added to the table.

Surface material	XPS N1s BE measured (eV)	XPS N1s peak BE from literature (eV)	Species
W	397.6 - 397.8	397.6 [12], 397.8 [12]	NH, surface nitride on W
	398.3 - 398.5	398.4 [11]	NH_2 on W
	400.4	400.7 [12]	second layer of adsorbed NH_3 on W
Cr	397.3 - 397.9	397 - 397.8 [48]	CrN
	398.3 - 398.9	398.6 [55]	NH_2 on Cr_2O_3/Cr
	399.1 - 399.5	399.0 - 399.8 [48]	CrN_xO_y
	400.4 - 401.0	400.7 [55]	NH_3 on Cr_2O_3/Cr
B	397.9	397.9 [56]	CN on B
	398.8 - 398.9	398.7 - 398.9 [46]	BN
	399.9 - 400.1	399.8 - 400.2 [57]	NH_2, NH on B
	401.7 - 401.9	401.7 - 402.1 [57]	NH_3 on B

The XPS measurements showed a continuous decomposition of NH_3 into NH_x (x = 0, 1 and 2) species, in agreement with previous studies done on W [11–14], B [58] and Cr [59]. The progressive dehydrogenation is schematized in Figure 6b, with NH_2, NH and N bound to the surface. As the number of H atoms bonded to the N atom is reduced, the adsorbed species move to a higher coordination site on the surface to maintain the valence of N.

5. Conclusion

In summary, NH_3 adsorption/desorption cycles performed on bare Au and on coated quartz crystals showed that the adsorption process is pressure and material dependent. The amount of NH_3 molecules bound to the surfaces was found to increase with increasing pressures for B, SS and W. Regarding Au and Be surfaces, a smaller number of ML was measured at higher pressures (500 to 800 mbar). No saturation was observed up to 800 mbar for W, B, and SS.

To explain the difference in the adsorption between materials, two types of interactions were presented. A strong adsorption on W, SS and B due to electron sharing between the NH_3 and the surface, leading to a true chemical bond. This strong interaction led also to the formation of multilayers through H bonds. In this case, the desorption of the gas was not complete and a continuous decomposition of the NH_3 on these surfaces was measured with XPS performed during several time intervals after the exposure.

On the other hand, a weak NH_3 adsorption is assumed on Au and Be and explained mainly by the H bond with O present on the surface. For those two materials, the desorption was complete according to QMB measurements and confirmed through XPS analysis.

6. Acknowledgements

This work has been carried out within the framework of the EUROfusion Consortium and has received funding from the Euratom research and training program 2014-2018 under grant agreement No 633053. The views and opinions expressed herein do not necessarily reflect those of the European Commission or of the ITER Organization. ITER is the Nuclear Facility INB no. 174. This paper applies new physics analysis related to tritiated ammonia formation which is not yet incorporated into the ITER technical baseline. The nuclear operator is not constrained by the results presented here. The authors would like to thank the Swiss Federal Office of Energy and the Federal Office for Education and Science for their financial support. We are also grateful to Sara Freund for the schematic figures of molecules on surfaces.

7. References

[1] R. Pitts, A. Kukushkin, A. Loarte, A. Martin, M. Merola, C. Kessel, V. Komarov, and M. Shimada, "Status and physics basis of the ITER divertor," *Physica Scripta*, vol. 2009, no. T138, p. 014001, 2009.

[2] A. Kallenbach, M. Bernert, R. Dux, L. Casali, T. Eich, L. Giannone, A. Herrmann, R. McDermott, A. Mlynek, H. Müller *et al.*, "Impurity seeding for tokamak power exhaust: from present devices via ITER to DEMO," *Plasma Physics and Controlled Fusion*, vol. 55, no. 12, p. 124041, 2013.

[3] J. Schweinzer, A. Sips, G. Tardini, P. Schneider, R. Fischer, J. Fuchs, O. Gruber, J. Hobirk, A. Kallenbach, R. McDermott *et al.*, "Confinement of improved H-modes in the all-tungsten ASDEX Upgrade with nitrogen seeding," *Nuclear Fusion*, vol. 51, no. 11, p. 113003, 2011.

[4] C. Giroud, G. Maddison, S. Jachmich, F. Rimini, M. Beurskens, I. Balboa, S. Brezinsek, R. Coelho, J. Coenen, L. Frassinetti *et al.*, "Impact of nitrogen seeding on confinement and power load control of a high-triangularity JET ELMy H-mode plasma with a metal wall," *Nuclear fusion*, vol. 53, no. 11, p. 113025, 2013.

[5] D. Neuwirth, V. Rohde, T. Schwarz-Selinger, and A. U. Team, "Formation of ammonia during nitrogen-seeded discharges at ASDEX Upgrade," *Plasma Physics and Controlled Fusion*, vol. 54, no. 8, p. 085008, 2012.

[6] V. Rohde, M. Oberkofler *et al.*, "Ammonia production in nitrogen seeded plasma discharges in ASDEX Upgrade," *Journal of Nuclear Materials*, vol. 463, pp. 672–675, 2015.

[7] J. Van Helden, W. Wagemans, G. Yagci, R. Zijlmans, D. Schram, R. Engeln, G. Lombardi, G. Stancu, and J. Röpcke, "Detailed study of the plasma-activated catalytic generation of ammonia in N_2-H_2 plasmas," *Journal of applied physics*, vol. 101, no. 4, p. 043305, 2007.

[8] M. Sode, W. Jacob, T. Schwarz-Selinger, and H. Kersten, "Measurement and modeling of neutral, radical, and ion densities in H_2-N_2-Ar plasmas," *Journal of Applied Physics*, vol. 117, no. 8, p. 083303, 2015.

[9] G. De Temmerman, M. Baldwin, D. Anthoine, K. Heinola, A. Jan, I. Jepu, J. Likonen, C. Lungu, C. Porosnicu, and R. Pitts, "Efficiency of thermal outgassing for tritium retention measurement and removal in ITER," *Nuclear Materials and Energy*, 2016.

[10] J. Winter, "Wall conditioning of fusion devices by reactive plasmas," *Journal of Nuclear Materials*, vol. 161, no. 3, pp. 265–330, 1989.

[11] C. Egawa, S. Naito, and K. Tamaru, "Adsorption and decomposition of ammonia on W (100); XPS and UPS studies," *Surface science*, vol. 131, no. 1, pp. 49–60, 1983.

[12] M. Grunze, C. Brundle, and D. Tomanek, "Adsorption and decomposition of ammonia on a W(110) surface: photoemission fingerprinting and interpretation of the core level binding energies using the equivalent core approximation," *Surface Science*, vol. 119, no. 2-3, pp. 133–149, 1982.

[13] P. Dawson and R. S. Hansen, "Field-Emission Study of the Adsorption and Decomposition of Ammonia on Tungsten," *The Journal of Chemical Physics*, vol. 48, no. 2, pp. 623–636, 1968.

[14] D. Masson, R. Merrill, and P. Houston, "The sticking and dissociation of NH_3 on W (110): a three-state model," *Surface science*, vol. 330, no. 3, pp. 239–254, 1995.

[15] P. Estrup and J. Anderson, "Adsorption and Decomposition of Ammonia on a Single-Crystal Tungsten (100) Surface," *The Journal of Chemical Physics*, vol. 49, no. 2, pp. 523–528, 1968.

[16] A. Bilić, J. R. Reimers, N. S. Hush, and J. Hafner, "Adsorption of ammonia on the gold (111) surface," *The Journal of chemical physics*, vol. 116, no. 20, pp. 8981–8987, 2002.

[17] A. Allouche, "Nitrogen reactivity toward beryllium: surface reactions," *Journal of Physics: Condensed Matter*, vol. 25, no. 22, p. 225002, 2013.

[18] A. de Castro, D. Alegre, and F. Tabarés, "Physisorption of ammonia on AISI 304L stainless steel at different surface temperature under high vacuum conditions," *Nuclear Materials and Energy*, vol. 9, pp. 1–5, 2016.

[19] A. Anghel, I. Mustata, C. Porosnicu, and C. Lungu, "Influence of the bias voltage on the formation of beryllium films by a thermionic vacuum arc method," *Journal of Nuclear Materials*, vol. 385, no. 2, pp. 242–245, 2009.

[20] S. Doniach and M. Sunjic, "Many-electron singularity in X-ray photoemission and X-ray line spectra from metals," *Journal of Physics C: Solid State Physics*, vol. 3, no. 2, p. 285, 1970.

[21] D. A. Shirley, "High-resolution X-ray photoemission spectrum of the valence bands of gold," *Physical Review B*, vol. 5, no. 12, p. 4709, 1972.

[22] R. Hesse, T. Chassé, and R. Szargan, "Peak shape analysis of core level photoelectron spectra using UNIFIT for WINDOWS," *Fresenius' journal of analytical chemistry*, vol. 365, no. 1, pp. 48–54, 1999.

[23] J. Scofield, "Hartree-Slater subshell photoionization cross-sections at 1254 and 1487 eV," *Journal of Electron Spectroscopy and Related Phenomena*, vol. 8, no. 2, pp. 129–137, 1976.

[24] G. Sauerbrey, "Use of quartz crystal units for weighing thin films and microweighing," *Magzine for Physics*, vol. 155, no. 2, pp. 206–222, 1959.

[25] C. Stockbridge, "Effects of gas pressure on quartz crystal microbalances," *Vacuum Microbalance Techniques*, vol. 5, pp. 147–178, 1966.

[26] K. K. Kanazawa and J. G. Gordon, "The oscillation frequency of a quartz resonator in contact with liquid," *Analytica Chimica Acta*, vol. 175, pp. 99–105, 1985.

[27] V. Tsionsky, L. Daikhin, M. Urbakh, and E. Gileadi, "Behavior of quartz crystal microbalance in nonadsorbed gases at high pressures," *Langmuir*, vol. 11, no. 2, pp. 674–678, 1995.

[28] Y.-T. Wu, P.-J. Akoto-Ampaw, M. Elbaccouch, M. L. Hurrey, S. L. Wallen, and C. S. Grant, "Quartz crystal microbalance (QCM) in high-pressure carbon dioxide (CO_2): Experimental aspects of QCM theory and CO_2 adsorption," *Langmuir*, vol. 20, no. 9, pp. 3665–3673, 2004.

[29] I. Kulchytskyy, M. G. Kocanda, and T. Xu, "Direct mass determination of hydrogen uptake using a quartz crystal microbalance," *Applied Physics Letters*, vol. 91, no. 11, p. 113507, 2007.

[30] L. Daikhin and M. Urbakh, "Effect of surface film structure on the quartz crystal microbalance response in liquids," *Langmuir*, vol. 12, no. 26, pp. 6354–6360, 1996.

[31] M. Urbakh and L. Daikhin, "Influence of the surface morphology on the quartz crystal microbalance response in a fluid," *Langmuir*, vol. 10, no. 8, pp. 2836–2841, 1994.

[32] M. Urbakh and L. Daikhin, "Roughness effect on the frequency of a quartz-crystal resonator in contact with a liquid," *Physical Review B*, vol. 49, no. 7, p. 4866, 1994.

[33] W. Plazinski, W. Rudzinski, and A. Plazinska, "Theoretical models of sorption kinetics including a surface reaction mechanism: A review," *Advances in Colloid and Interface Science*, vol. 152, no. 1, pp. 2 – 13, 2009.

[34] P. M. Gundry and F. C. Tompkins, "Chemisorption of gases on metals," *Q. Rev. Chem. Soc.*, vol. 14, pp. 257–291, 1960.

[35] N. Surplice and W. Brearley, "The adsorption of carbon monoxide, ammonia, and wet air on gold," *Surface Science*, vol. 52, no. 1, pp. 62–74, 1975.

[36] M. E. Coltrin and B. D. Kay, "Quasiclassical trajectory study of rotational energy transfer in the scattering of NH_3 from a flat, rigid gold surface," *The Journal of chemical physics*, vol. 89, no. 1, pp. 551–561, 1988.

[37] R. Richton and L. Farrow, "Adsorption kinetics of ammonia on an inhomogeneous gold surface," *The Journal of Physical Chemistry*, vol. 85, no. 24, pp. 3577–3581, 1981.

[38] B. D. Kay, K. R. Lykke, J. R. Creighton, and S. J. Ward, "The influence of adsorbate–absorbate hydrogen bonding in molecular chemisorption: NH_3, HF, and H_2O on Au (111)," *The Journal of chemical physics*, vol. 91, no. 8, pp. 5120–5121, 1989.

[39] A. Tsyganenko, D. Pozdnyakov, and V. Filimonov, "Infrared study of surface species arising from ammonia adsorption on oxide surfaces," *Journal of Molecular Structure*, vol. 29, no. 2, pp. 299–318, 1975.

[40] D. Jennison, P. Schultz, and M. Sears, "Ab initio calculations of adsorbate hydrogen-bond strength: ammonia on Pt (111)," *Surface science*, vol. 368, no. 1-3, pp. 253–257, 1996.

[41] K. Jacobi, Y. Wang, C. Y. Fan, and H. Dietrich, "Adsorption and thermal dehydrogenation of ammonia on Ru (1121)," *The Journal of Chemical Physics*, vol. 115, no. 9, pp. 4306–4313, 2001.

[42] J. Parmeter, Y. Wang, C. Mullins, and W. Weinberg, "Electron energy loss spectroscopy of ammonia on Ru (001)," *The Journal of chemical physics*, vol. 88, no. 8, pp. 5225–5236, 1988.

[43] K. Manandhar, W. Walkosz, Y. Ren, S. Otani, P. Zapol, and M. Trenary, "Structure and Reactivity of Molecularly Adsorbed Ammonia on the ZrB_2(0001) Surface," *The Journal of Physical Chemistry C*, vol. 118, no. 50, pp. 29 260–29 269, 2014.

[44] B. Diawara, L. Joubert, D. Costa, P. Marcus, and C. Adamo, "Ammonia on Ni (111) surface studied by first principles: Bonding, multilayers structure and comparison with experimental IR and XPS data," *Surface Science*, vol. 603, no. 20, pp. 3025–3034, 2009.

[45] M. C. Wu, C. M. Truong, and D. W. Goodman, "Interactions of ammonia with a nickel oxide (100) surface studied by high-resolution electron energy loss spectroscopy and temperature programmed desorption spectroscopy," *The Journal of Physical Chemistry*, vol. 97, no. 16, pp. 4182–4186, 1993.

[46] E. Il'inchik and I. Merenkov, "X-ray photoelectron study of the effect of the composition of the initial gas phase on changes in the electronic structure of hexagonal boron nitride films obtained by PECVD from borazine," *Journal of Structural Chemistry*, vol. 57, no. 4, pp. 670–678, 2016.

[47] I. Caretti and I. Jiménez, "Influence of carbon content and nitrogen vacancies on the bonding structure and mechanical performance of graphite-like BC $_x$n thin films," *Journal of Applied Physics*, vol. 112, no. 6, p. 063525, 2012.

[48] A. Lippitz and T. Hübert, "XPS investigations of chromium nitride thin films," *Surface and Coatings Technology*, vol. 200, no. 1, pp. 250–253, 2005.

[49] M. Romand and M. Roubin, "Esca (Electron Spectroscopy for Chemical Analysis) Studies of Chromium and Vanadium Nitrides," *Analusis*, vol. 4, no. 7, pp. 308–312, 1976.

[50] R. Haasch, T.-Y. Lee, D. Gall, J. Greene, and I. Petrov, "Epitaxial CrN (001) Grown and Analyzed In situ by XPS and UPS. i. Analysis of As-deposited Layers," *Surface Science Spectra*, vol. 7, no. 3, pp. 250–261, 2000.

[51] D. K. Nandi, U. K. Sen, S. Sinha, A. Dhara, S. Mitra, and S. K. Sarkar, "Atomic layer deposited tungsten nitride thin films as a new lithium-ion battery anode," *Physical Chemistry Chemical Physics*, vol. 17, no. 26, pp. 17 445–17 453, 2015.

[52] K. Schmid, A. Manhard, C. Linsmeier, A. Wiltner, T. Schwarz-Selinger, W. Jacob, and S. Mändl, "Interaction of nitrogen plasmas with tungsten," *Nuclear Fusion*, vol. 50, no. 2, p. 025006, 2010.

[53] B. Eren, L. Marot, I. Ryzhkov, S. Lindig, A. Houben, M. Wisse, O. Skoryk, M. Oberkofler, V. Voitsenya, C. Linsmeier *et al.*, "Roughening and reflection performance of molybdenum coatings exposed to a high-flux deuterium plasma," *Nuclear fusion*, vol. 53, no. 11, p. 113013, 2013.

[54] Y. Zhao, W. Hu, Y. Xia, E. Smith, Y. Zhu, C. Dunnill, and D. Gregory, "Preparation and characterization of tungsten oxynitride nanowires," *Journal of materials chemistry*, vol. 17,

no. 41, pp. 4436–4440, 2007.

[55] H. Ma, Y. Berthier, and P. Marcus, "AES, XPS, and TDS study of the adsorption and desorption of NH_3 on ultra-thin chromium oxide films formed on chromium single crystal surfaces," *Applied surface science*, vol. 153, no. 1, pp. 40–46, 1999.

[56] M. Alcala, J. Sanchez-Lopez, C. Real, A. Fernandez, and P. Matteazzi, "Mechanosynthesis of carbon nitride compounds," *Diamond and related materials*, vol. 10, no. 11, pp. 1995–2001, 2001.

[57] X. Gouin, P. Grange, L. Bois, P. L'Haridon, and Y. Laurent, "Characterization of the nitridation process of boric acid," *Journal of alloys and compounds*, vol. 224, no. 1, pp. 22–28, 1995.

[58] J. A. Rodriguez, C. M. Truong, and D. W. Goodman, "Synthesis of boron nitride ultrathin films: The bonding and chemistry of ammonia and hydrazine on Ru (0001) and B/Ru (0001) surfaces," *Journal of Vacuum Science & Technology A: Vacuum, Surfaces, and Films*, vol. 10, no. 4, pp. 955–959, 1992.

[59] H. Cheng, D. B. Reiser, P. M. Mathias, K. Baumert, and S. W. Dean Jr, "Investigation of nitriding mechanism at transition metal surfaces: NH_3 Adsorption and Decomposition on Fe (100), Ni (100), and Cr (100)," *The Journal of Physical Chemistry*, vol. 99, no. 11, pp. 3715–3722, 1995.